5-1-2017

Biplane Fluoroscopy for Hindfoot Motion Analysis during Gait: A Model-based Evaluation

Janelle A. Cross
Medical College of Wisconsin

Ben McHenry
Marquette University, ben.mchenry@marquette.edu

Robert C. Molthen
Marquette University, robert.molthen@marquette.edu

Emily Exten
Meriter Unity Point

Taly Gilat-Schmidt
Marquette University, tal.gilat-schmidt@marquette.edu

See next page for additional authors

Biplane fluoroscopy for hindfoot motion analysis during gait: A model-based evaluation

Janelle A. Cross
Department of Orthopaedic Surgery, Medical College of Wisconsin
Milwaukee, WI

Benjamin D. McHenry
Department of Biomedical Engineering, Marquette University
Milwaukee, WI

Robert Molthen
Department of Biomedical Engineering, Marquette University
Milwaukee, WI

Emily Exten
Orthopaedic Surgery, Meriter UnityPoint
Monona, WI

Taly Gilat Schmidt
Department of Biomedical Engineering, Marquette University

[Medical Engineering & Physics, Vol 43, (May 2017): pg. 118-123. DOI.

Milwaukee, WI

Gerald F. Harris

Department of Biomedical Engineering, Marquette University
Milwaukee, WI

Abstract: The purpose of this study was to quantify the accuracy and precision of a biplane fluoroscopy system for model-based tracking of *in vivo* hindfoot motion during over-ground gait. Gait was simulated by manually manipulating a cadaver foot specimen through a biplane fluoroscopy system attached to a walkway. Three 1.6-mm diameter steel beads were implanted into the specimen to provide marker-based tracking measurements for comparison to model-based tracking. A CT scan was acquired to define a gold standard of implanted bead positions and to create 3D models for model-based tracking. Static and dynamic trials manipulating the specimen through the capture volume were performed. Marker-based tracking error was calculated relative to the gold standard implanted bead positions. The bias, precision, and root-mean-squared (RMS) error of model-based tracking was calculated relative to the marker-based measurements. The overall RMS error of the model-based tracking method averaged 0.43 ± 0.22 mm and $0.66 \pm 0.43°$ for static and 0.59 ± 0.10 mm and $0.71 \pm 0.12°$ for dynamic trials. The model-based tracking approach represents a non-invasive technique for accurately measuring dynamic hindfoot joint motion during *in vivo*, weight bearing conditions. The model-based tracking method is recommended for application on the basis of the study results.

Keywords: Biplane fluoroscopy; Model-based;Hindfoot; Gait; Biomechanics

1. Introduction

Gait analysis is commonly used to evaluate lower extremity kinematics and kinetics of both normal and pathological motion patterns. Conventionally, external markers are placed on the skin over specific bony landmarks, such that optical cameras can track marker locations and relate them to the motion of the underlying bones [1]. This method has been well documented and is frequently used in research and clinical studies [2,3]. While optical motion analysis systems are easy to implement and are clinically relevant for multiple applications, methodological shortcomings affect analyses of the hindfoot. Understanding the biomechanics of the hindfoot during gait is critical to the proper care of patients with a variety of orthopedic impairments and foot deformities resulting from conditions such as cerebral palsy, spina bifida, clubfoot, traumatic brain injury and spinal cord injury [4].

The foot consists of 26 bones, many of which lack suitable landmarks for external marker placement. In current external marker based models, individual bones are frequently grouped together in segments. The most simplistic models treat the entire foot as a single segment with a single "ankle" joint, while more complex multi-segmental models divide the foot among two to nine segments [4–10]. Only the nine segment model developed by Hwang et al. included individual segments of the calcaneus and talus to allow for subtalar joint motion to be determined [9]. In all of these models, bones within a segment are assumed not to move with respect to each other. This "rigid-segment" assumption has been questioned in the literature, with errors as high as 6.9° reported [11]. In addition to the methodological requirement of grouping bones together, external marker based models suffer from skin motion artifact (SMA). SMA is the relative movement between a skin mounted marker and the underlying bone and is considered the most significant source of error in gait analysis [1,12]. In the hindfoot, SMA has been reported to range from 2.7 to 14.9 mm, with the largest error occurring at the malleoi [13].

Fluoroscopy offers a valuable complement to conventional motion analysis by providing dynamic intra-articular joint motion measurements during weight bearing while eliminating rigid-body assumptions and SMA. The radiographic nature of fluoroscopy also allows for gait analysis during shoe wear, brace wear, and orthotic usage that is not achievable using optical motion analysis with external

markers. Two-dimensional (2D) *in vivo* fluoroscopic analysis of the hindfoot has been reported by both our group and other authors [14–22]. While these 2D analyses are valuable for quantifying single plane dynamics, they lack the ability to determine out of plane motions, such as axial rotation of the subtalar joint [23,24]. Capturing tri-axial motion requires the addition of a second fluoroscope to capture images in two different planes. The radiographic image sequences are required to be captured synchronously to enable accurate three-dimensional (3D) localization of the bone segments at each time point.

Biplane fluoroscopy is performed with two different tracking techniques. In marker-based tracking, tantalum beads implanted in bones are used to track and calculate kinematics. A minimum of three beads per bone segment are required for 3D analysis [25]. This is an invasive procedure that is limited to animals, or subjects who are undergoing a surgical procedure at the same time as implantation [26]. Model-based tracking determines bone position and orientation by comparing a 3D bone model, obtained with a CT or MR scan, to the acquired biplane fluoroscopic images [27]. Model based tracking is non-invasive, and with properly defined protocols, result in minimal dose of ionizing radiation.

For biplane systems, it is recommended that an evaluation be performed specifically for the anatomical joints and activities that it will be used to analyze [28,29]. The majority of bi-plane foot/ankle studies appearing in the literature analyzed quasi-static motions [30–34], not natural gait. Of the dynamic foot/ankle studies found in the literature, accuracy was either not reported [35,36], or assumed to be the same as that of systems designed for other anatomical joints [30,37]. One recently reported biplane study does describe sub-millimeter precision and accuracy in a system specifically designed for analysis of the foot/ankle during gait [38]. In that study, the gait cycle was determined in a piecewise manner, as the use of a treadmill prevented heel strike and toe off data from being collected simultaneously. Another biplane system designed for the foot also describing sub-millimeter precision was validated using four articulated, and two unarticulated dry tarsal bones recording at 15 Hz [39]. The goal of the current study was to evaluate the static and dynamic error of a biplane system designed for analyzing *in vivo* hindfoot motion during over-ground gait using a model-based tracking

algorithm. Marker-based tracking was additionally evaluated and used as the control when determining accuracy of model-based tracking, similar to previously performed studies [26,29,40,41].

2. Methods

2.1. Biplane system

The biplane system (Fig. 1) was constructed to be centered about a 46.4 by 50.8 cm force plate (AMTI OR6-500 6-DOF, Watertown, MA) embedded in a 7 m long custom walkway. Two x-ray sources (OEC 9000, GE Healthcare, Fairfield, CT), and two image intensifiers (II's, 15" diam., Dunlee, Aurora, IL) were custom mounted to the walkway with a 60° angle between the sources. The source-to-detector and source-to-object-center distances were 112 cm and 76 cm, respectively for both source-intensifier pairs. During data acquisition, the x-ray sources were set at 100 kV and 2.0 mA continuous exposure, with an estimated effective dose of 10 μSv during a 2 s trial. High-speed, high resolution (1024 × 1024) cameras (N4, IDT, Pasadena, CA) with 52 mm lenses (Nikon, Melville, NY) were attached to each II. Images were captured at 200 fps and digitized directly to a controller PC via Motion Studio 64 (Version 2.10.05, IDT, Pasadena, CA). A trigger mechanism was developed to ensure synchronous recording between the cameras and the force plate. High acceleration impact testing was performed to ensure accurate, simultaneous detection of heel strike and toe off in the fluoroscopic images. A superball was dropped on the force plate so that only a single fluoroscopic frame (at 200 fps) with the ball in contact appeared. This was then compared with a single frame spike in the analog force plate data at the same time (±1 frame).

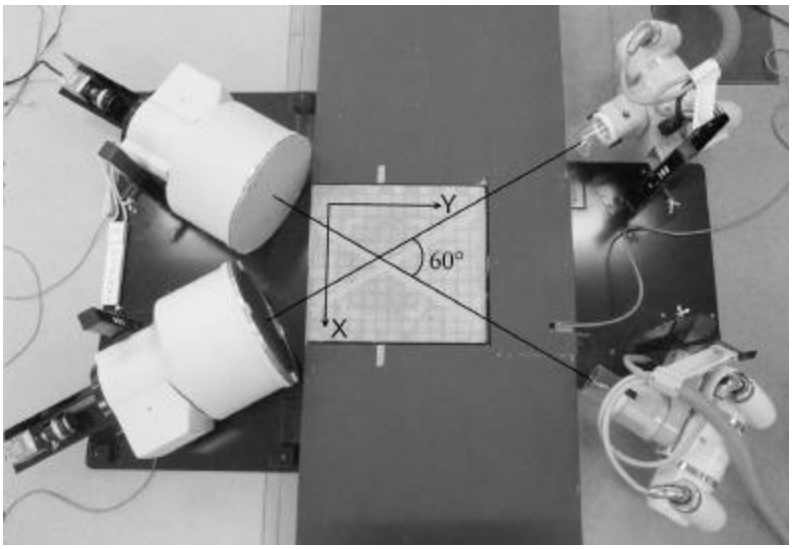

1. Download high-res image (411KB)
2. Download full-size image

Fig. 1. Custom built biplane fluoroscopic system attached to walkway with embedded force plate; *x*- and *y*-axis of lab coordinate system shown (z-axis pointing up).

2.2. Cadaver specimen

A fresh frozen trans-tibial cadaver foot from a 34 year old male was obtained in accordance with institutionally approved IRB standards. Three 1.6-mm diameter steel beads were implanted into each of the three hindfoot bones (calcaneus, talus, and tibia) with minimal dissection of the surrounding soft tissues, and maximal distance between beads in the same bone (Fig. 2). A board eligible orthopedic surgeon drilled 2-mm holes into the cortical bone so that the beads could be manually pressed into the hole until flush according to the method described by Bey et al. [26]. The beads were then secured into place using cyanoacrylate adhesive. A 16-mm diameter steel rod was fixed to the specimen using a bone plate attached to the proximal end of the tibia for manual manipulation through the imaging capture volume.

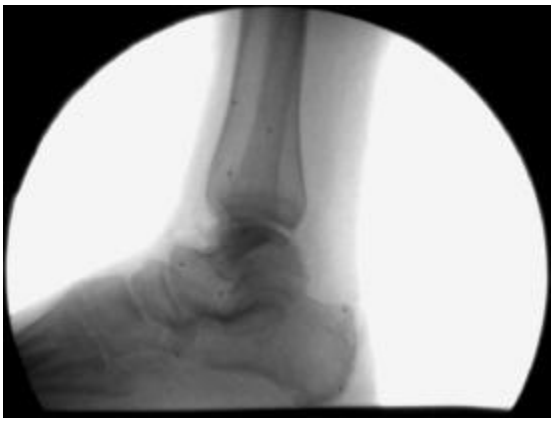

1. Download high-res image (74KB)
2. Download full-size image

Fig. 2. Fluoroscopic image of the nine bead positions within the cadaver specimen.

2.3. CT scan

A CT scan (120 kV, 270 mA) of the cadaver foot was obtained consisting of 956, 0.625-mm thick transverse-plane slices (512 × 512 pixels) (LightSpeed VCT, GE Healthcare, Milwaukee, WI) to generate volumetric models of the calcaneus, talus, and tibia. An image processing algorithm was implemented in MATLAB (MathWorks, Natick, MA) to determine the sub-pixel bead centroids, which represented the gold standard bead locations. For model-based tracking, 3D bone models were generated by segmentation of the CT scan performed using 32-bit OsiriX software (version 3.8.1, Pixmeo, Geneva, Switzerland). Within the 3D bone models, the radiopaque bead locations were identified manually and replaced with the mean values from surrounding voxels to eliminate influences of the beads on the model-based tracking.

2.4. Static and dynamic trials

Image sequences were obtained during 33 different static positions of the foot (100 frames per trial), as well as during 10 dynamic trials (150–200 frames per trial). Rotational static positions were captured at 11 different foot progression angles, in 5° rotational

increments from −25° to +25°, with the heel placed at the center of the capture volume (Fig. 3A). Translational static positions were collected with a neutral foot progression angle at 22 positions within the capture volume in accordance to a 30 × 30 cm grid (Fig. 3B). Finally, 10 dynamic trials were collected by manually simulating gait through the volume via the attached tibial rod. The force plate was used for event detection of heel strike and toe off.

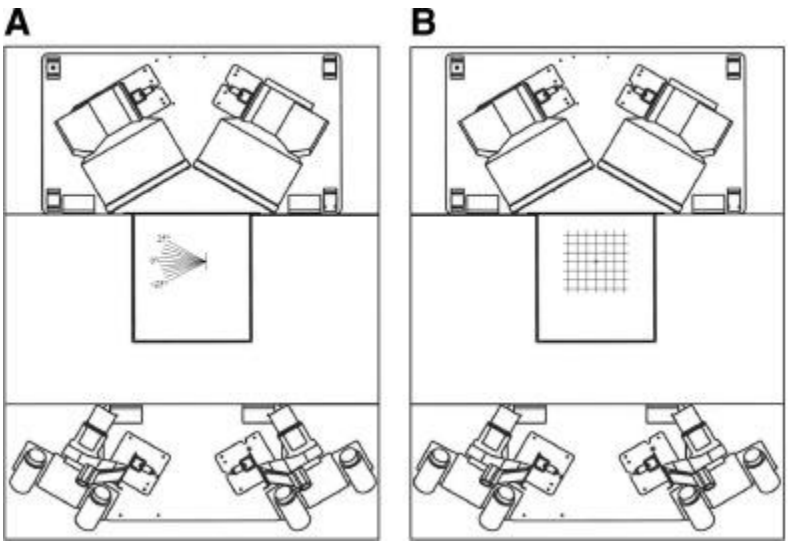

1. Download high-res image (283KB)
2. Download full-size image

Fig. 3. (A) 11 static foot progression angles. (B) Grid used for translational measurements.

2.5. Distortion correction and geometry calibration

Open source software, X-Ray Reconstruction of Moving Morphology (XROMM, Brown University, Providence, RI) was used for II distortion correction as described by Brainerd et al. [25]. The direct linear transformation (DLT) technique was used to define the linear transformation between the 3D object space and the 2D image planes [42]. An acrylic calibration cube with 64 precisely positioned steel spheres implanted as calibration points [25] was manufactured and imaged with the biplane system. A coordinate measuring machine (CMM, Gage 2000, Brown & Sharpe, North Kingstown, RI) was used to document the physical geometrical characteristics of the cube, and to

verify the positions of the beads within a linear accuracy of 0.005 mm. Points in the x-ray images of the cube were digitized and compared with the known points of the cube, as measured by the CMM, to determine the 11 DLT coefficients [43]. The calibration cube origin was used as the global lab coordinate system origin, with the *x*-axis parallel to walkway, *y*-axis across the walkway, and *z*-axis (vertical) perpendicular to the walkway (*x*- and *y*-axis shown in Fig. 1).

2.6. Marker-based tracking

After image distortion correction and geometry calibration, marker-based tracking was performed using standard DLT techniques [43]. In the first image of each sequence, the implanted beads were manually selected to start the automated tracking algorithm. If the algorithm failed to locate a bead while tracking the sequence, the bead was relocated manually, and then the automated tracking was resumed. The Euclidean distance between two beads within the same bone was found in both the CT and fluoroscopic images. The CT inter-bead distance was considered the true distance. The marker-based tracking error was calculated as the absolute value of the true distance minus the estimated distance. Error was calculated within each image, with the mean and standard deviation reported for the entire sequence, for all of the trials, as previously done in similar validation studies [25,44–46].

2.7. Model-based tracking

The acquired static and dynamic fluoroscopic imaging sequences were also used to quantify the accuracy and precision of model-based tracking. An automated image processing algorithm located the beads in all the 2D fluoroscopic images and replaced the bead pixels with intensity values from the distribution of pixels in the region surrounding each bead prior to model-based tracking. Model-based tracking was performed using validated software, Autoscoper (Brown University, Providence, RI) [44]. Autoscoper follows the auto-registration algorithms developed by You et al. [27] and Bey et al. [26]. These algorithms use digitally reconstructed radiographs (DRRs) generated by ray-traced projections through a 3D bone model. Autoscoper uses a downhill simplex optimization algorithm that

iterates over the 6 degree of freedom (DOF) motion parameters to find the bone positions for which the DRRs best match the acquired x-ray images. In the current study, the calcaneus, tibia, and talus were tracked separately using 3D bone models generated from the CT data. A trained user first manually aligned the bone models with the biplane x-ray images to obtain the best visual fit every 2 to 5 frames throughout the image sequence. Sobel edge detection and contrast enhancement filters were applied to the bone models and biplane image sequences to improve alignment. These parameters were selected by the user to provide the best visual match. The Autoscoper optimization algorithm was then performed on the manually aligned frames, with the Autoscoper software interpolating between the optimized frames. Once the tracking was complete, the 6 DOF results were output (*x, y, z* position, yaw, pitch, roll orientation from the origin of the CT scan) with respect to the lab coordinate system.

Accuracy of the trials was assessed by simultaneously comparing marker-based and model-based tracking results. The marker-based tracking directly found the bead locations in the lab coordinate system. Model-based tracking found the bone position (6 DOF) of the CT origin in the lab coordinate system. With the known bead positions from the CT scan, a transformation matrix was applied to the Autoscoper output to project the 3D positions of the beads in the laboratory coordinate system, to enable a direct comparison between the marker-based and model-based tracking translational error (in millimeters). To determine the rotational error, the three bead locations in each bone were used to create local coordinate systems. A YXZ Euler angle sequence was used to compare the rotational differences between the marker-based and model-based output of each bone. Agreement between the marker-based and model-based tracking results was quantified as bias in each xyz bead coordinate (difference in bead positions between the two methods, averaged across all trials) and precision (standard deviation of the difference in bead positions between the two methods, averaged across all trials). The root-mean-squared (RMS) error of the bead positions estimated through model-based tracking relative to the marker-based bead positions across all trials was calculated to assess the overall accuracy of the model-based tracking method. To assess the intra-observer error associated with the model-based tracking

method, all three bones were tracked repeatedly five times in one randomly selected dynamic trial.

3. Results

The marker-based tracking method resulted in an average of 0.1% error across the three bones in both the static and dynamic trials. The absolute error was lower in the static trials than the dynamic trials for all three bones, with the differences ranging from 0.05 to 0.10 mm (Table 1).

Table 1. Marker-based absolute mean tracking error (reported in mm) and standard deviation (± SD).

	Calcaneus	**Talus**	**Tibia**	**Overall**
Static	0.16 ± 0.04	0.14 ± 0.05	0.13 ± 0.04	0.15 ± 0.04
Dynamic	0.22 ± 0.12	0.19 ± 0.15	0.23 ± 0.18	0.21 ± 0.15

The overall bias, precision, and RMS error for the static, dynamic and intra-observer trials all demonstrated sub-millimeter and sub-degree tracking results. The model-based tracking bias, precision, and RMS error results are listed in Table 2. The overall precision and RMS error were both lower in the static trials than the dynamic, with the translational error smaller than rotational error across all trials (Table 2). The overall RMS error between methods averaged 0.43 ± 0.22 mm and 0.66 ± 0.43° for static trials, and 0.59 ± 0.10 mm and 0.71 ± 0.12° for dynamic trials. Across all trials, the tibia had the lowest RMS error, followed by the talus, then the calcaneus. The intra-observer error of model-based tracking was low across all three measures, with an overall RMS error between trials of 0.62 ± 0.12 mm and 0.66 ± 0.14° (Table 3).

Table 2. Model-based tracking accuracy for individual bones (± SD).

	Calcaneus	**Talus**	**Tibia**	**Overall**
(A) Model-based tracking bias				
Static (mm)	−0.08 ± 0.28	0.13 ± 0.45	0.05 ± 0.22	0.03 ± 0.32

	Calcaneus	Talus	Tibia	Overall
Static (°)	0.10 ± 0.69	−0.05 ± 0.95	0.02 ± 0.65	0.02 ± 0.76
Dynamic (mm)	−0.16 ± 0.17	−0.04 ± 0.22	−0.09 ± 0.15	−0.10 ± 0.18
Dynamic (°)	0.13 ± 0.20	0.02 ± 0.28	0.01 ± 0.26	0.06 ± 0.25
(B) Model-based tracking precision				
Static (mm)	0.09 ± 0.08	0.06 ± 0.03	0.05 ± 0.03	0.07 ± 0.05
Static (°)	0.06 ± 0.03	0.33 ± 0.14	0.13 ± 0.06	0.17 ± 0.08
Dynamic (mm)	0.86 ± 0.24	0.51 ± 0.08	0.40 ± 0.07	0.59 ± 0.13
Dynamic (°)	0.69 ± 0.15	0.68 ± 0.11	0.66 ± 0.08	0.67 ± 0.11
(C) Model-based tracking RMS				
Static (mm)	0.54 ± 0.23	0.47 ± 0.27	0.26 ± 0.16	0.43 ± 0.22
Static (°)	0.56 ± 0.40	0.88 ± 0.55	0.55 ± 0.32	0.66 ± 0.43
Dynamic (mm)	0.84 ± 0.16	0.52 ± 0.09	0.42 ± 0.06	0.59 ± 0.10
Dynamic (°)	0.72 ± 0.15	0.72 ± 0.12	0.68 ± 0.10	0.71 ± 0.12

Table 3. Intra-observer error of model-based tracking (± SD).

	Calcaneus	Talus	Tibia	Overall
(A) Intra-observer bias, precision, RMS (mm)				
Bias	−0.01 ± 0.08	0.00 ± 0.35	0.01 ± 0.07	0.00 ± 0.17
Precision	0.93 ± 0.13	0.63 ± 0.21	0.56 ± 0.09	0.71 ± 0.14
RMS error	0.75 ± 0.10	0.57 ± 0.17	0.52 ± 0.08	0.62 ± 0.12
(B) Intra-observer bias, precision, RMS (°)				
Bias	−0.05 ± 0.16	0.02 ± 0.12	0.06 ± 0.09	0.01 ± 0.12
Precision	0.64 ± 0.11	0.58 ± 0.18	0.62 ± 0.10	0.61 ± 0.13
RMS error	0.66 ± 0.10	0.61 ± 0.21	0.71 ± 0.09	0.66 ± 0.14

4. Discussion

This study evaluated the static and dynamic error of a biplane fluoroscopic system using both marker-based and model-based tracking of the hindfoot during over-ground gait. For marker-based tracking, the system's average absolute error across all three bones was 0.15 ± 0.04 mm for static and 0.21 ± 0.15 mm for dynamic trials. These numbers compare well with marker-based validation in other systems (Table 4). The previous marker-based studies evaluated their systems using phantom objects with implanted metal beads that may not replicate complex bone geometries. The current study used beads implanted in bones in a cadaver specimen with all the soft tissues intact. This allowed for a realistic system evaluation under the same conditions that would be used to clinically analyze hindfoot kinematics. In addition, the purpose of the marker-based tracking was to establish a control reference in which to compare the model-based tracking, as model-based is the objective moving forward to avoid the invasive implanting of beads in human subjects.

Table 4. Summary of marker-based validation study results.

	Static translation	**Static rotation**	**Dynamic**
Miranda et al. [43]	0.12 mm (±0.08)	0.09° (±0.08)	–
Iaquinto et al. [44]	0.094 mm (±0.081)	0.083° (±0.068)	0.126 mm (±0.122)
Tashman et al. [45]	–	–	0.02 mm
Brainerd et al. [25]	–	–	0.037 mm (±0.046)

For model-based tracking, current study results indicated that the system had a bias range of −0.16 to 0.13 mm and −0.05 to 0.13°, precision range of 0.05 to 0.86 mm and 0.06 to 0.69°, and an overall dynamic RMS average error of 0.59 mm and 0.71°. In both the static and dynamic trials, the tibia had the lowest RMS error, followed by the talus, then the calcaneus. This same order of error across the three bones was also found by Wang et al. for both the bias and precision measures [38]. Wang et al. found a bias range of 0.31 mm–0.50 mm

and a precision range of 0.15 mm–0.20 mm in their system [38]. It is hypothesized that the long bone shape of the tibia is easier to track than the irregular shape of the talus and calcaneus.

The extremely low intra-observer user error demonstrates the highly repeatability method of the semi-automated model-based tracking technique used. The intra-observer user error bias of 0.00 ± 0.17 mm and $0.01 \pm 0.12°$ was similar to findings of Anderst et al. reported from repeatedly tracking two cervical spine segments three times using model-based tracking (0.02 mm and 0.06°) [47].

Although approximately 5000 frames were used to track the bones, the study was limited by using a single cadaver specimen. The use of a cadaver specimen was essential in the validation of the model-based tracking method, due to the limitations and invasiveness of implanting markers into human subjects. The system has been previously used as a 2D, sagittal plane system to analyze 13 subjects hindfoot kinematics during barefoot ambulation [16,17]. This study is additionally limited by the use of ionizing radiation. The effective dose during a foot and ankle CT scan is 70 μSv, which is slightly less than the 80 μSv of effective dose received from a conventional chest x-ray [48]. The effective dose for a foot and ankle CT, plus 1 biplane fluoroscopic static trial and 10 dynamic trials in the current system is estimated to total 180 μSv. The United States Nuclear Regulatory Commission places an annual occupational limit of whole body effective dose at 5 rems (50,000 μSv). In the United States, the average person is exposed to 3000 μSv every year from natural background radiation [49]. To reduce radiation exposure, the use of MRI [30,40] or statistical shape models [50,51] could be investigated to eliminate the CT scan.

Numerous factors that may influence the accuracy of model-based tracking, including the shape of a particular bone, the method used during CT segmentation of the bone, the radiographic parameters (voltage and current), the presence of surrounding soft tissues, the overlap from surrounding bones, the magnitude of joint motion, and the velocity of joint motion [29]. Because of these factors, it is important that each system be evaluated specifically for the anatomical joints and activities for which it will be used [28,29]. In the current study on hindfoot motion during gait, the overall dynamic RMS

average error of 0.59 mm is well below the estimated 2.7–14.9 mm error at the foot due to skin movement artifacts of skin-mounted markers [13]. These results indicate that biplanar fluoroscopic hardware and tracking methods can be used to effectively track *in vivo* hindfoot bone motion within 0.59 mm and 0.71°. In this study, model-based tracking was evaluated under the conditions that match the planned *in vivo* tracking trials.

Conflict of interest

Taly Gilat Schmidt receives research funding from GE Healthcare. Janelle A. Cross, Benjamin D. McHenry, Robert Molthen, Emily Exten, and Gerald F. Harris have no conflicts of interest to disclose.

Acknowledgments

The contents of this paper were developed under a grant from the Department of Education, NIDRR grant number H133E100007. However, those contents do not necessarily represent the policy of the Department of Education, and you should not assume endorsement by the Federal Government.

References:

[1]
A. Cappozzo, F. Catani, A. Leardini, M. Benedetti, U. Della Croce**Position and orientation in space of bones during movement: experimental artefacts**
Clin Biomech, 11 (1996), pp. 90-100
ArticlePDF (1MB)

[2]
A. Cappozzo, T. Leo, A. Pedotti**A general computing method for the analysis of human locomotion**
J Biomech, 8 (1975), pp. 307-320
ArticlePDF (1MB)

[3]
M.P. Kadaba, H.K. Ramakrishnan, M.E. Wootten**Measurement of lower extremity kinematics during level walking**
J Orthop Res, 8 (1990), pp. 383-392

[4]

S.M. Kidder, F.S. Abuzzahab Jr., G.F. Harris, J.E. Johnson**A system for the analysis of foot and ankle kinematics during gait**
IEEE Trans Rehabil Eng, 4 (1996), pp. 25-32

[5]

A. Leardini, M.G. Benedetti, F. Catani, L. Simoncini, S. Giannini**An anatomically based protocol for the description of foot segment kinematics during gait**
Clin Biomech, 14 (1999), pp. 528-536
ArticlePDF (316KB)

[6]

M.C. Carson, M.E. Harrington, N. Thompson, J.J. O'Connor, T.N. Theologis**Kinematic analysis of a multi-segment foot model for research and clinical applications: a repeatability analysis**
J Biomech, 34 (2001), pp. 1299-1307
ArticlePDF (380KB)

[7]

A.E. Hunt, R.M. Smith, M. Torode, A. Keenan**Inter-segment foot motion and ground reaction forces over the stance phase of walking**
Clin Biomech, 16 (2001), pp. 592-600
ArticlePDF (199KB)

[8]

B.A. MacWilliams, M. Cowley, D.E. Nicholson**Foot kinematics and kinetics during adolescent gait**
Gait Posture, 17 (2003), pp. 214-224
ArticlePDF (661KB)

[9]

S.J. Hwang, H.S. Choi, Y.H. Kim**Motion analysis based on a multi-segment foot model in normal walking**
2004 IEMBS '04 26th Annual International Conference of the IEEE, 2, Engineering in Medicine and Biology Society (2004), pp. 5104-5106

[10]

T.R. Jenkyn, A.C. Nicol**A multi-segment kinematic model of the foot with a novel definition of forefoot motion for use in clinical gait analysis during walking**
J Biomech, 40 (2007), pp. 3271-3278

ArticlePDF (325KB)

[11]

C.J. Nester, A.M. Liu, E. Ward, D. Howard, J. Cocheba, T. Derrick**Error in the description of foot kinematics due to violation of rigid body assumptions**
J Biomech, 43 (2010), pp. 666-672
ArticlePDF (874KB)

[12]

A. Leardini, L. Chiari, U.D. Croce, A. Cappozzo**Human movement analysis using stereophotogrammetry: Part 3. Soft tissue artifact assessment and compensation**
Gait Posture, 21 (2005), pp. 212-225
ArticlePDF (253KB)

[13]

B.A. Maslen, T.R. Ackland**Radiographic study of skin displacement errors in the foot and ankle during standing**
Clin Biomech, 9 (1994), pp. 291-296
ArticlePDF (715KB)

[14]

B. McHenry, J. Long, G.F. Harris**Foot and ankle motion analysis using dynamic radiographic (fluoroscopic) imaging**
Proceedings of the Galt and Clinical Movement Analysis Society (2012), pp. 181-182

[15]

McHenry B.**Foot and ankle motion analysis using dynamic radiographic imaging**
Dissertation, Marquette University, Milwaukee, WI (2013)

[16]

B.D. McHenry, E.L. Exten, J. Long, B. Law, R.M. Marks, G. Harris**Sagittal subtalar and talocrural joint assessment with weight-bearing fluoroscopy during barefoot ambulation**
Foot Ankle Int., 36 (4) (2015), pp. 430-435

[17]

B.D. McHenry, E. Exten, J.T. Long, G.F. Harris**Sagittal fluoroscopy for the assessment of hindfoot kinematics**
J Biomech Eng, 138 (2016), Article 034502

[18]

S. Yamaguchi, T. Sasho, H. Kato, Y. Kuroyanagi, S.A. Banks**Ankle and subtalar kinematics during dorsiflexion-plantarflexion activities**
Foot Ankle Int, 30 (2009), pp. 361-366

[19]
T. Kobayashi, Y. No, K. Yoneta, M. Sadakiyo, K. Gamada**In vivo kinematics of the talocrural and subtalar joints with functional ankle instability during weight-bearing ankle internal rotation: a pilot study**
Foot Ankle Spec, 6 (2013), pp. 178-184

[20]
T. Kobayashi, M. Saka, E. Suzuki, N. Yamazaki, M. Suzukawa, A. Akaike, *et al.***In vivo kinematics of the talocrural and subtalar joints during weightbearing ankle rotation in chronic ankle instability**
Foot Ankle Spec, 7 (2014), pp. 13-19

[21]
M. Fukano, T. Fukubayashi**Changes in talocrural and subtalar joint kinematics of barefoot versus shod forefoot landing**
J Foot Ankle Res, 7 (2014), p. 42, 10.1186/s13047-014-0042-9

[22]
M. Fukano, Y. Kuroyanagi, T. Fukubayashi, S.A. Banks**Three-dimensional kinematics of the talocrural and subtalar joints during drop landing**
J Appl Biomech, 30 (2014), pp. 160-165

[23]
S.A. Banks, W.A. Hodge**Accurate measurement of three-dimensional knee replacement kinematics using single-plane fluoroscopy**
IEEE Trans Biomed Eng, 43 (1996), pp. 638-649

[24]
M.R. Mahfouz, W.A. Hoff, R.D. Komistek, D.A. Dennis**A robust method for registration of three-dimensional knee implant models to two-dimensional fluoroscopy images**
IEEE Trans Med Imaging, 22 (2003), pp. 1561-1574

[25]
E.L. Brainerd, D.B. Baier, S.M. Gatesy, T.L. Hedrick, K.A. Metzger, S.L. Gilbert, *et al.***X-ray reconstruction of moving**

morphology (XROMM): precision, accuracy and applications in comparative biomechanics research
J Exp Zool Part A: Ecol Gen Physiol, 313A (2010), pp. 262-279

[26]
M.J. Bey, R. Zauel, S.K. Brock, S. Tashman**Validation of a new model-based tracking technique for measuring three-dimensional, in vivo glenohumeral joint kinematics**
J Biomech E, 128 (2006), 10.1115/1.2206199

[27]
B.M. You, P. Siy, W. Anderst, S. Tashman**In vivo measurement of 3-D skeletal kinematics from sequences of biplane radiographs: application to knee kinematics**
IEEE Trans Med Imaging, 20 (2001), pp. 514-525

[28]
S. Tashman**Comments on "validation of a non-invasive fluoroscopic imaging technique for the measurement of dynamic knee joint motion"**
J Biomech, 41 (2008), pp. 3290-3291
ArticlePDF (164KB)

[29]
M.J. Bey, S.K. Kline, S. Tashman, R. Zauel**Accuracy of biplane x-ray imaging combined with model-based tracking for measuring in-vivo patellofemoral joint motion**
J Orthop Surg Res, 3 (2008), 10.1186/1749-799X-3-38

[30]
R.J. de Asla, L. Wan, H.E. Rubash, G. Li**Six DOF in vivo kinematics of the ankle joint complex: application of a combined dual-orthogonal fluoroscopic and magnetic resonance imaging technique**
J Orthop Res, 24 (2006), pp. 1019-1027

[31]
G. Li, L. Wan, M. Kozanek**Determination of real-time in-vivo cartilage contact deformation in the ankle joint**
J Biomech, 41 (2008), pp. 128-136
ArticlePDF (629KB)

[32]
L. Wan, R.J. de Asla, H.E. Rubash, G. Li**In vivo cartilage contact deformation of human ankle joints under full body weight**

J Orthop Res, 26 (2008), pp. 1081-1089

[33]

R. de Asla, M. Kozanek, L. Wan, H. Rubash, G. Li**Function of anterior talofibular and calcaneofibular ligaments during in-vivo motion of the ankle joint complex**
J Orthop Surg Res, 4 (2009), p. 7, 10.1186/1749-799X-4-7

[34]

A.M. Caputo, J.Y. Lee, C.E. Spritzer, M.E. Easley, J.K. DeOrio, J.A. Nunley, *et al.***In vivo kinematics of the tibiotalar joint after lateral ankle instability**
Am J Sports Med, 37 (2009), pp. 2241-2248

[35]

C.D. Peltz, J.A. Haladik, S.E. Hoffman, M. McDonald, N.L. Ramo, G. Divine, *et al.***Effects of footwear on three-dimensional tibiotalar and subtalar joint motion during running**
J Biomech, 47 (2014), pp. 2647-2653
ArticlePDF (2MB)

[36]

S. Koo, K.M. Lee, Y.J. Cha**Plantar-flexion of the ankle joint complex in terminal stance is initiated by subtalar plantar-flexion: a bi-planar fluoroscopy study**
Gait Posture, 42 (2015), pp. 424-429
ArticlePDF (1020KB)

[37]

K.J. Campbell, K.J. Wilson, R.F. LaPrade, T.O. Clanton**Normative rearfoot motion during barefoot and shod walking using biplane fluoroscopy**
Knee Surg Sports Traumatol Arthros, 24 (4) (2016), pp. 1402-1408

[38]

B. Wang, K.E. Roach, A.L. Kapron, N.M. Fiorentino, C.L. Saltzman, M. Singer, *et al.***Accuracy and feasibility of high-speed dual fluoroscopy and model-based tracking to measure in vivo ankle arthrokinematics**
Gait Posture, 41 (2015), pp. 888-893
ArticlePDF (953KB)

[39]

K. Ito, K. Hosoda, M. Shimizu, S. Ikemoto, S. Kume, T. Nagura, *et al.***Direct assessment of 3D foot bone kinematics using**

biplanar X-ray fluoroscopy and an automatic model registration method
J Foot Ankle Res, 8 (2015), p. 21, 10.1186/s13047-015-0079-4

[40]
G. Li, S.K. Van de Velde, J.T. Bingham**Validation of a non-invasive fluoroscopic imaging technique for the measurement of dynamic knee joint motion**
J Biomech, 41 (2008), pp. 1616-1622
ArticlePDF (574KB)

[41]
W.J. Anderst, R. Zauel, J. Bishop, E. Demps, S. Tashman**Validation of three-dimensional model-based tibio-femoral tracking during running**
Med Eng Phys, 31 (2009), pp. 10-16
ArticlePDF (378KB)

[42]
L. Chen, C.W. Armstrong, D.D. Raftopoulos**An investigation on the accuracy of three-dimensional space reconstruction using the direct linear transformation technique**
J Biomech, 27 (1994), pp. 493-500
ArticlePDF (760KB)

[43]
T.L. Hedrick**Software techniques for two- and three-dimensional kinemtic measurements of biological an biomimetic systems**
Bioinspiration Biomimetics, 3 (3) (2008), 10.1088/1748-3182/3/3/034001

[44]
D.L. Miranda, J.B. Schwartz, A.C. Loomis, E.L. Brainerd, B.C. Fleming, J.J. Crisco**Static and dynamic error of a biplanar videoradiography system using marker-based and markerless tracking techniques**
J Biomech Eng, 133 (2011), Article 121002

[45]
J.M. Iaquinto, R. Tsai, D.R. Haynor, M.J. Fassbind, B.J. Sangeorzan, W.R. Ledoux**Marker-based validation of a biplane fluoroscopy system for quantifying foot kinematics**

Med Eng Phys, 36 (2014), pp. 391-396
ArticlePDF (850KB)

[46]
S. Tashman, W. Anderst**In-vivo measurement of dynamic joint motion using high speed biplane radiography and CT: application to canine ACL deficiency**
J Biomech Eng, 125 (2003), pp. 238-245

[47]
W.J. Anderst, E. Baillargeon, W.F. Donaldson III, J.Y. Lee, J.D. Kang**Validation of a noninvasive technique to precisely measure in vivo three-dimensional cervical spine movement**
Spine, 36 (2011), pp. E393-E400

[48]
D. Biswas, J.E. Bible, M. Bohan, A.K. Simpson, P.G. Whang, J.N. Grauer**Radiation exposure from musculoskeletal computerized tomographic scans**
J Bone Joint Surg, 91 (2009), pp. 1882-1889

[49]
D.J. Brenner, R. Doll, D.T. Goodhead, E.J. Hall, C.E. Land, J.B. Little, *et al.***Cancer risks attributable to low doses of ionizing radiation: Assessing what we really know**
Proc Natl Acad Sci, 100 (2003), pp. 13761-13766

[50]
N. Baka, B.L. Kaptein, J.E. Giphart, M. Staring, Md. Bruijne, B.P.F. Lelieveldt, *et al.***Evaluation of automated statistical shape model based knee kinematics from biplane fluoroscopy**
J Biomech, 47 (2014), pp. 122-129
ArticlePDF (2MB)

[51]
M. Valenti, E. De Momi, W. Yu, G. Ferrigno, M. Akbari Shandiz, C. Anglin, *et al.***Fluoroscopy-based tracking of femoral kinematics with statistical shape models**
Int J Comput Assist Radiol Surg, 11 (2016), pp. 757-765